

# Bio-inspired Collision-free 4D Trajectory Generation for UAVs Using Tau Strategy

Zuqiang Yang, Zhou Fang, Ping Li

*School of Aeronautics and Astronautics, Zhejiang University, Hangzhou 310027, China*

---

## Abstract

Inspired by the general tau theory in animal motion planning, a collision-free four-dimensional (4D) trajectory generation method is presented for multiple Unmanned Aerial Vehicles (UAVs). This method can generate a group of optimal or near-optimal collision-free 4D trajectories, the position and velocity of which are synchronously planned in accordance with the arrival time. To enlarge the shape adjustment capability of trajectories with zero initial acceleration, a new strategy named intrinsic tau harmonic guidance strategy is proposed on the basis of general tau theory and harmonic motion. In the case of multiple UAVs, the 4D trajectories generated by the new strategy are optimized by the bionic Particle Swarm Optimization (PSO) algorithm. In order to ensure flight safety, the protected airspace zone is used for collision detection, and two collision resolution approaches are applied to resolve the remaining conflicts after global trajectory optimization. Numerous simulation results of the simultaneous arrival missions demonstrate that the proposed method can effectively provide more flyable and safer 4D trajectories than that of the existing methods.

**Keywords:** bio-inspired, 4D trajectory generation, general tau theory, multiple UAVs

Copyright © 2016, Jilin University. Published by Elsevier Limited and Science Press. All rights reserved.

doi: 10.1016/S1672-6529(14)60162-1

---

## 1 Introduction

Unmanned Aerial Vehicles (UAVs) play important roles in time-critical cooperative missions such as simultaneous attack<sup>[1]</sup>, cooperative surveillance<sup>[2]</sup>, and formation flight<sup>[3]</sup>. In these missions, the members of a UAV group need to arrive at the destinations simultaneously or on schedule. The applications of four-dimensional (4D) trajectory, which adds a precise time dimension into the three-dimensional (3D) trajectory, can lower the uncertainty of trajectories and improve the reliability of mission execution. Hence further study of 4D trajectory generation is required to deal with the challenging time-critical missions.

Recent researches of 4D trajectory generation mainly concentrate on the airport terminal approaching management in civil aviation<sup>[4–6]</sup>, but the achievements for UAVs are limited. Most of the existing 4D trajectory generation methods for UAVs use the mathematical expression to describe the position-time relation of a trajectory<sup>[7–11]</sup>, such as Bezier polynomial function<sup>[9]</sup> and pseudospectral method<sup>[10]</sup>. The other kind of methods

are graph search techniques like A\* algorithm<sup>[12]</sup> which are preferred to solve the NP-hard trajectory generation problem<sup>[13]</sup>. However, several disadvantages make these conventional methods inappropriate for 4D trajectory generation of UAVs. Firstly, most of the conventional methods rely on speed assignments for 3D trajectories to meet the arrival time. Hence these methods are not specially designed for 4D tasks, and the discontinuity of setting speed will cause the loss of tracking accuracy. Secondly, the trajectory descriptions of most existing methods are so complex that the trajectory optimization for multi-UAVs is computationally expensive.

To overcome the disadvantages of the conventional methods, researchers have tried to study the planning mechanism of animals and utilize bio-inspired approach in trajectory generation. Recently, the bio-inspired general tau theory has received great interest. This theory is developed from the action planning mechanism of animals such as gannets fishing<sup>[14]</sup>, pigeons landing<sup>[15]</sup>, and flare maneuver of pilots<sup>[16]</sup>. Based on the general tau theory, several Intrinsic Tau Guidance Strategies (ITGSs)<sup>[17,18]</sup> are specially proposed for 4D motion

---

**Corresponding author:** Zhou Fang

**E-mail:** zfang@zju.edu.cn

guidance. According to the arrival time, these strategies can synchronously plan the time-variant position and velocity with more succinct expressions. Considering this advantage, researchers have used the ITGSs in the motion planning of single UAV, such as the braking, docking, landing<sup>[19,20]</sup>, perching like a bird<sup>[21]</sup>, and the rapid point-to-point movement<sup>[18]</sup>. However, because of two drawbacks, little research has applied the ITGSs in multi-UAV scenarios. Firstly, the ITGS guided by gravity (tau-G strategy)<sup>[17]</sup>, which is most commonly used in UAV fields, provides guidance with a non-zero initial acceleration. Due to dynamic constraints, the UAV starting from rest cannot exactly track the trajectory generated by tau-G strategy. Secondly, the small trajectory shape adjustment area of the existing ITGSs limits the collision resolution capability in trajectory generation for multi-UAVs.

The main contribution of our work is twofold. Firstly, combining the bio-inspired general tau theory with the property of harmonic motion, we propose a new strategy named intrinsic tau harmonic guidance strategy (tau-H strategy). The 4D trajectory generated by this strategy not only has the zero initial acceleration, but also achieves a stronger shape adjustment capability for de-confliction. Secondly, a comprehensive collision-free 4D trajectory generation method based on the tau-H strategy is presented for multi-UAVs. This method utilizes the tau-H strategy to generate 4D trajectories, and applies the modified Particle Swarm Optimization (PSO) to optimize the trajectory generation problem. To ensure flight safety, the method applies the ellipsoidal Protected Airspace Zone (PAZ)<sup>[22]</sup> to detect potential collisions. For the remaining collisions after global trajectory optimization, two Collision Resolution (CR) approaches are adopted to resolve the problem efficiently. Numerous simulations of the simultaneous arrival missions are carried out to demonstrate that the proposed method can effectively generate more flyable and safer 4D trajectories than the existing methods.

The remainder of this paper is organized as follows. In section 2, the collision-free 4D trajectory generation problem of multiple UAVs is stated. In section 3, we propose the tau-H strategy. Then the whole 4D trajectory generation method is described in section 4. Section 5 presents the simulation results and analysis in contrast with other methods. The final section gives the conclusion and our future work.

## 2 Problem statement

The problem considered in this paper is concerned in cooperative missions like simultaneous attack and formation initialization. For this problem, the proposed method should generate a group of collision-free and optimal 4D trajectories which can guide multiple UAVs moving from arbitrary initial positions to their destinations exactly at the arrival time  $T$ . A 4D trajectory in the navigation frame  $\mathbf{N}$  ( $O, X, Y, Z$ ) is described by the time-variant state set  $\mathcal{S}(t)=\{X(t), Y(t), Z(t), v_X(t), v_Y(t), v_Z(t)\}$ , in which  $(X(t), Y(t), Z(t))$  and  $(v_X(t), v_Y(t), v_Z(t))$  denote the time-variant 3D positions and velocities respectively.

The architecture of 4D trajectory generation for  $N_{\text{UAV}}$  UAVs is shown in Fig. 1. The input information contains the initial states  $\bigcup_{i=1}^{N_{\text{UAV}}} \mathcal{S}_i(t_0)$  from the vehicles, and the arrival time, the goal states  $\bigcup_{i=1}^{N_{\text{UAV}}} \mathcal{S}_i(t_0+T)$  and the constraints from the task planner. The constraints include the collision-free requirement, the arrival time, the maximum velocity  $v_{\max}$ , and the maximum acceleration  $a_{\max}$ . According to the input information, the 4D trajectory generation method optimizes the trajectories, detects and resolves collisions, and outputs the flyable and optimal trajectories for UAVs.

## 3 The intrinsic tau harmonic strategy

### 3.1 General tau theory

When animals want to approach the targets, their motions are guided by the remaining Time to Contact (TTC). Lee proposed the tau theory<sup>[23]</sup>, which pointed that a visual variable named tau ( $\tau$ ) could provide the information of TTC for animals. The tau variable is defined as the ratio of the distance and the relative movement velocity between the animal and its target<sup>[15]</sup>.

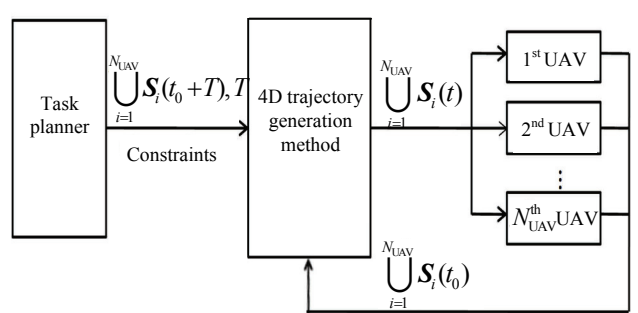


**Fig. 1** Schematic diagram of 4D trajectory generation for UAVs.

Afterwards, Lee presented the general tau theory<sup>[17]</sup>. In this theory, the tau variable is generalized to the TTC of transition from the current motion state to the goal state, and the goal of the motion is to close the gap  $\chi$  between two states. The definition of  $\tau_\chi(t)$  at time  $t$  is shown in Eq. (1),

$$\tau_\chi(t) = \begin{cases} \frac{\chi(t)}{\dot{\chi}(t)} & |\dot{\chi}(t)| \geq \dot{\chi}_{\min} \\ \tau_{\min} & |\dot{\chi}(t)| < \dot{\chi}_{\min} \end{cases}. \quad (1)$$

As  $\tau_\chi(t)$  is set negative in the closure of  $\chi$ , it should be limited to  $\tau_{\min}$  as  $\dot{\chi} \rightarrow 0$ . With the help of general tau theory, the tau variable becomes an exciting tool for the goal-directed motion planning of UAV. In 4D trajectory generation, the motion gap  $\chi$  can be the gap of any state in  $S(t)$ , for instance,  $\tau_x(t)$ ,  $\tau_y(t)$  and  $\tau_z(t)$  are the tau variables of 3D position gaps.

### 3.2 Existing ITGSs

The ITGSs are designed on the basis of the tau coupling strategy, which is inspired by the catching and intercepting motions of animals<sup>[17]</sup>. The tau coupling strategy is that if different motion gaps need to be closed together, their tau variables should be kept in non-zero constant ratios during the closure of these gaps. Furthermore, a virtual gap called the intrinsically generated gap can be designed for movement guidance. The strategy which couples the actual movement gap with the intrinsically generated gap is named the ITGS. The most commonly used ITGS is the tau-G strategy, whose intrinsically generated gap  $G(t)$  is the free fall movement with gravity. The expressions of  $G(t)$  and  $\tau_G(t)$  are shown in Eq. (2),

$$\begin{cases} G(t) = \frac{1}{2}g(T^2 - t^2) \\ \tau_G(t) = \frac{G(t)}{\dot{G}(t)} = \frac{1}{2}(t - \frac{T^2}{t}) \end{cases}. \quad (2)$$

The relations between tau variables of 3D position gaps and  $\tau_G(t)$  are shown in Eq. (3),

$$\begin{cases} \tau_x(t) = k_x \tau_G(t) \\ \tau_y(t) = k_y \tau_G(t), \\ \tau_z(t) = k_z \tau_G(t) \end{cases} \quad (3)$$

where, non-zero constants  $k_x$ ,  $k_y$  and  $k_z$  are called the coupling coefficients.

Take the closure along  $X$ -axis as an example, the  $X$ -axis gap is  $x(t) = X(T) - X(t)$ . Substituting  $x(t) / \dot{x}(t)$  for  $\tau_x(t)$  in Eq. (3), the expressions of gap, velocity and acceleration ( $x(t)$ ,  $\dot{x}(t)$ ,  $\ddot{x}(t)$ ) can be obtained as shown in Eq. (4) by solving  $\tau_x(t) = k_x \tau_G(t)$ ,

$$\begin{cases} x(t) = \frac{x_0}{T^{\frac{2}{k_x}}} (T^2 - t^2)^{\frac{1}{k_x}} \\ \dot{x}(t) = \frac{-2x_0 t}{k_x T^{\frac{3}{k_x}}} (T^2 - t^2)^{\frac{1-k_x}{k_x}} \\ \ddot{x}(t) = \frac{2x_0}{k_x T^{\frac{3}{k_x}}} \left( \frac{2-k_x}{k_x} t^2 - T^2 \right) (T^2 - t^2)^{\frac{1-2k_x}{k_x}} \end{cases}. \quad (4)$$

Fig. 2 shows the relations between  $(x(t), \dot{x}(t), \ddot{x}(t))$  and  $k_x$  with  $x_0 = 10$  m and  $T = 5$  s. If  $k_x \in (0, 0.5)$ ,  $x(t), \dot{x}(t), \ddot{x}(t) \rightarrow 0$  when  $t \rightarrow T$ . In addition, the initial acceleration  $\ddot{x}(0)$  is non-zero, which indicates that the initial acceleration is discontinuous if the UAV starts from rest or a hovering state. Hence the 4D trajectory generated by tau-G strategy is hard to be tracked exactly due to the dynamic constraints of UAV.

To overcome this drawback, Zhang *et al.* proposed the tau jerk (tau-J) guidance strategy<sup>[18]</sup>, which uses the movement  $J(t)$  with a constant jerk  $j$  as the intrinsically generated gap.  $J(t)$  and the acceleration  $\ddot{x}(t)$  guided by this strategy are shown in Eq. (5),

$$\begin{cases} J(t) = \frac{1}{6}j(T^3 - t^3) \\ \ddot{x}(t) = \frac{3x_0 t}{k_x T^{\frac{3}{k_x}}} \left( \frac{3-k_x}{k_x} t^3 - 2T^3 \right) (T^3 - t^3)^{\frac{1-2k_x}{k_x}} \end{cases}. \quad (5)$$

Except for the zero initial acceleration, the other features of tau-J strategy are similar to those of tau-G strategy. Unfortunately, the small trajectory shape adjustment area is still a limitation of tau-J strategy for multi-UAV applications.

### 3.3 Intrinsic tau harmonic strategy

The ITGSs commonly use the translational motion as the intrinsic guidance motion. Besides translational motion, harmonic motion is also a basic motion form in nature, such as the movement of a simple pendulum shown in Fig. 3. The harmonic motion is periodic, and

the velocity of the pendulum is sinusoidal if the ball starts moving from rest at the left or right side. Combining the feature of harmonic motion with the bio-inspired general tau theory, we present a new strategy called the intrinsic tau harmonic guidance strategy (tau-H strategy).

In tau-H strategy, the harmonic motion is used to describe the velocity of the intrinsic motion, which means the intrinsic motion has a sinusoidal acceleration. The expressions of the intrinsically generated gap  $H(t)$  and its derivatives are shown as

$$\begin{cases} H(t) = H_0 \left[ \frac{1}{2\pi} \sin\left(\frac{2\pi t}{T}\right) - \frac{t}{T} + 1 \right] \\ \dot{H}(t) = H_0 \left[ \frac{1}{T} \cos\left(\frac{2\pi t}{T}\right) - \frac{1}{T} \right] \\ \ddot{H}(t) = H_0 \left[ -\frac{2\pi}{T^2} \sin\left(\frac{2\pi t}{T}\right) \right] \end{cases}, \quad (6)$$

where,  $H_0$  is the initial value of  $H(t)$ .

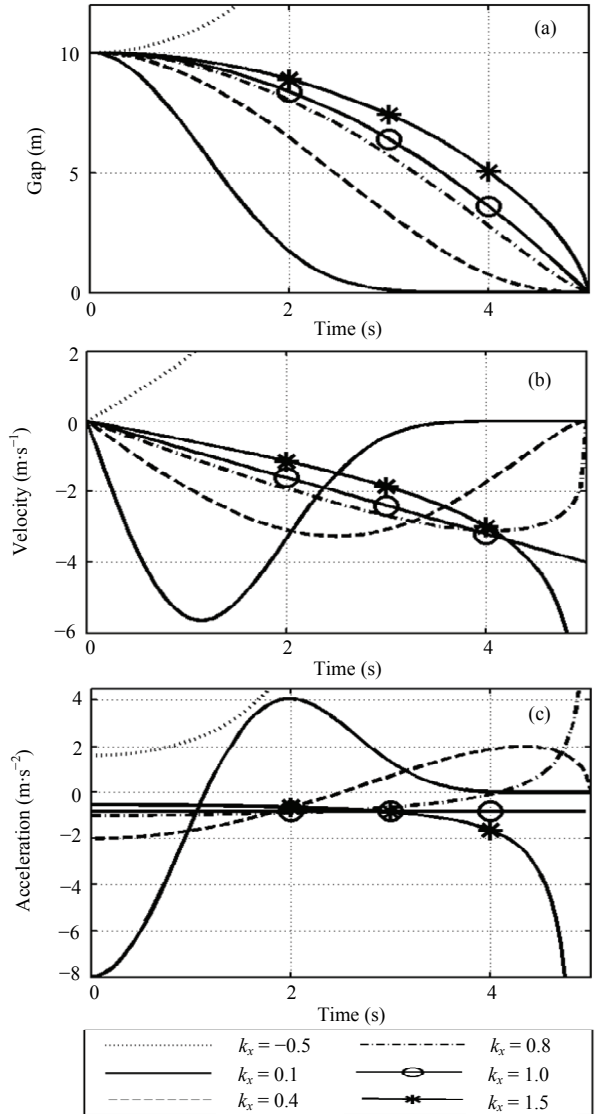
By solving  $\tau_x(t) = k_x \tau_H(t) = k_x H(t) / \dot{H}(t)$ , the expressions of  $(x(t), \dot{x}(t), \ddot{x}(t))$  can be obtained as

$$\begin{cases} x(t) = x_0 h^{\frac{1}{k_x}} \\ \dot{x}(t) = \frac{x_0}{k_x} \dot{h} h^{\frac{1-k_x}{k_x}} \\ \ddot{x}(t) = \frac{x_0}{k_x} h^{\frac{1-2k_x}{k_x}} \left( \frac{1-k_x}{k_x} \dot{h}^2 + h \ddot{h} \right) \end{cases}, \quad (7)$$

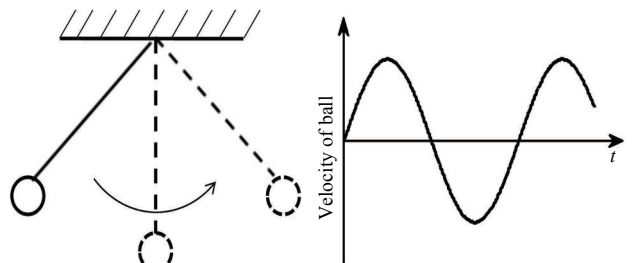
where,  $h$  represents  $H/H_0$ .

Fig. 4 shows the relations between  $(x(t), \dot{x}(t), \ddot{x}(t))$  and coefficient  $k_x$  with  $x_0 = 10$  m and  $T = 5$  s. It is easy to conclude that the acceleration at the initial moment is zero. This feature overcomes the drawback of the tau-G strategy. Therefore, the tau-H strategy can guide a UAV starting from rest steadily, moving toward the destination, and stopping there at the arrival time. Furthermore, we can find another important feature that if  $k_x \in (0, 1]$  and  $(x(t), \dot{x}(t), \ddot{x}(t))$  are calculated by Eq. (6) and Eq. (7),  $(x(t), \dot{x}(t), \ddot{x}(t)) \rightarrow 0$  when  $t \rightarrow T$ . This feature means the tau-H strategy can guarantee the steady closure of the state gap while doubling the value range of the coupling coefficient. A proof of this feature is given as follows.

From Eq. (6),  $H(t)$  and its derivatives are bounded,



**Fig. 2** Time-variant (a) gap, (b) velocity and (c) acceleration of tau-G strategy with different  $k_x$  values.



**Fig. 3** The harmonic motion and the sinusoidal velocity of a pendulum.

and when  $t \rightarrow T$ , one can obtain  $\lim_{t \rightarrow T} H(t) = 0$ ,  $\lim_{t \rightarrow T} \dot{H}(t) = 0$ , and  $\lim_{t \rightarrow T} \ddot{H}(t) = 0$ . So  $\lim_{t \rightarrow T} \ddot{h} = \lim_{t \rightarrow T} (\dot{H} / H_0) = 0$ .

If  $k_x \in (0, 1]$ ,  $\frac{1}{1-k_x}$  and  $(1-k_x)/k_x$  are positive. So  $\lim_{t \rightarrow T} h^{\frac{1}{k_x}} = 0$  and  $\lim_{t \rightarrow T} h^{\frac{k_x}{1-k_x}} = 0$ . According to the property of limits, it can be deduced that  $\lim_{t \rightarrow T} x(t) = 0$  and  $\lim_{t \rightarrow T} \dot{x}(t) = 0$ .

The expression of acceleration can be rewritten as:

$$\ddot{x}(t) = \frac{x_0}{k_x} h^{\frac{1-k_x}{k_x}} \left( \frac{1-k_x}{k_x} \frac{\dot{h}^2}{h} + \ddot{h} \right). \quad (8)$$

Substituting the expressions of  $H(t)$  and  $\dot{H}(t)$  into  $\dot{h}^2/h$ , one can obtain

$$\begin{aligned} \frac{\dot{h}^2}{h} &= \frac{1}{T^2} \frac{2\cos^2\theta - 2\cos\theta + \sin^2\theta}{\frac{1}{2\pi}\sin\theta - \frac{t-T}{T}} \\ &= \frac{2\cos\theta \frac{\cos\theta - 1}{\sin\theta} + \sin\theta}{T^2 \left( \frac{1}{2\pi} + \frac{T-t}{T\sin\theta} \right)}, \end{aligned} \quad (9)$$

where,  $\theta = 2\pi t/T$  when  $t \rightarrow T$  and  $\theta \rightarrow 2\pi$ .

Analyzing the different parts of Eq. (9) separately, their limits are shown in Eq. (10) because of  $\lim_{\theta \rightarrow 2\pi} \sin\theta = 0$  and  $\lim_{\alpha \rightarrow 0} \frac{\sin\alpha}{\alpha} = 0$ .

$$\begin{aligned} \lim_{\theta \rightarrow 2\pi} \frac{\cos\theta - 1}{\sin\theta} &= \lim_{\theta \rightarrow 0} \frac{-2\sin^2\frac{\theta}{2}}{2\sin\frac{\theta}{2}\cos\frac{\theta}{2}} = \lim_{\theta \rightarrow 0} \frac{-\sin\frac{\theta}{2}}{2\cos\frac{\theta}{2}} = 0 \\ \lim_{t \rightarrow T} \frac{T-t}{\sin\left(\frac{2\pi t}{T}\right)} &= -\frac{T}{2\pi} \lim_{t \rightarrow T} \frac{2\pi - \frac{2\pi t}{T}}{\sin\left(2\pi - \frac{2\pi t}{T}\right)} = \infty. \end{aligned} \quad (10)$$

According to Eq. (10),  $\lim_{t \rightarrow T} \frac{\dot{h}^2}{h} = 0$ . Considering  $\lim_{t \rightarrow T} \ddot{h} = 0$  and  $\lim_{t \rightarrow T} h^{\frac{1}{k_x}} = 0$ , we can deduce that  $\lim_{t \rightarrow T} \ddot{x}(t) = 0$  if  $k_x \in (0, 1]$ .

The above proof indicates that if  $k_x \in (0, 1]$ ,  $(x(t), \dot{x}(t), \ddot{x}(t)) \rightarrow 0$  when  $t \rightarrow T$ . It is important to note that the expansion of the value range of  $k_x$  may broaden the spatial adjustment area of the trajectories guided by the ITGSs. In 4D trajectory generation, the trajectory can be decomposed into 3D position gaps, which should be closed simultaneously. Eq. (11) shows the time-variant positions guided by the tau-H strategy.

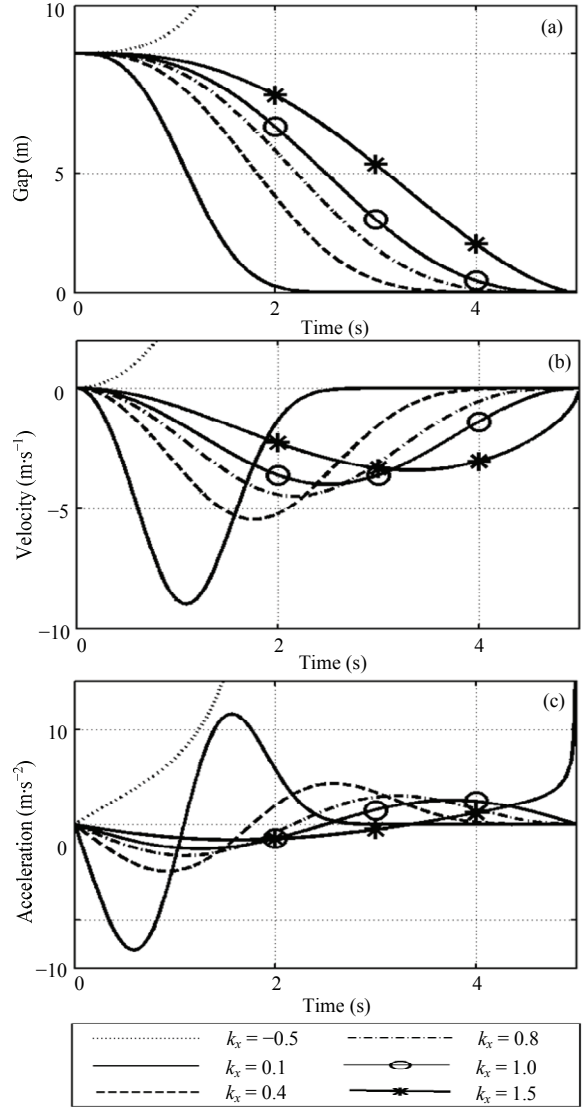


**Fig. 4** Time-variant (a) gap, (b) velocity and (c) acceleration of tau-H strategy with different  $k_x$  values.

$$\begin{cases} x_H(t) = x_0 h^{\frac{1}{k_x}} \\ y_H(t) = y_0 h^{\frac{1}{k_y}} \\ z_H(t) = z_0 h^{\frac{1}{k_z}} \end{cases} \quad (11)$$

To yield the spatial relations of trajectory, Eq. (11) can be rewritten as

$$\begin{cases} y_H = \frac{y_0}{x_0^{k_x/k_y}} x_H^{k_x/k_y} \\ z_H = \frac{z_0}{x_0^{k_x/k_z}} x_H^{k_x/k_z} \end{cases} \quad (12)$$

Because  $x_H \in [0, x_0]$ , the 3D shape of the trajectory is determined by the coupling coefficient set  $\mathbf{k} = \{k_x, k_y, k_z\}$ . According to Eqs. (2) and (5), the movements guided by tau-G and tau-J strategies have the same spatial relations as Eq. (12). Consequently, with the same coefficient set  $\mathbf{k}$ , the trajectories generated by different tau guidance strategies have identical spatial shapes in 3D space. As a result, given the same  $k_x$ , the 4D trajectory can be adjusted in a larger space if the ranges of  $k_y$  and  $k_z$  are expanded.

To illustrate the difference of trajectory shape adjustment capability between tau-H strategy and the existing ones, the two-dimensional trajectories with  $k_x = 0.25$  and different  $k_y$  values are shown in Fig. 5. The task parameters include  $x_0 = 5$  m,  $y_0 = 5$  m and  $T = 5$  s. The trajectory adjustment area of the tau-H strategy is larger than that of others, and the trajectory shapes of different strategies are identical with the same  $k_y$ . For the existing tau strategies, if a highly curved trajectory is needed,  $k_y$  should be chosen close to zero. However, the coefficient can be set near one by using tau-H strategy. According to Refs. [18, 20] and Fig. 4, the maximum velocity of the three strategies along Y-axis is larger if the  $k_y$  is closer to zero. Hence the tau-H strategy can provide the highly curved trajectory with a smaller maximum velocity than other tau strategies. This feature is very useful for collision avoidance in trajectory generation of multi-UAVs with the maximum velocity constraints.

#### 4 The collision-free 4D trajectory generation method for UAVs

For the applications of multi-UAVs, the 4D trajectories generated by tau-H strategy are optimized by the modified PSO algorithm. So the presented trajectory generation method is called tau-H-PSO for short. The flow diagram of tau-H-PSO is shown in Fig. 6. In the beginning, a global PSO is conducted to obtain the optimal coupling coefficient set  $\mathbf{k}^*$  of the trajectories. The global trajectory shape adjustment by optimizing  $\mathbf{k}$  can avoid most of the collisions. If no collision is detected, the generation is accomplished. But in some challenging missions, collisions are still existent when PSO meets the maximum number of iterations. In such cases, two CR approaches are sequentially applied to resolve the remaining collisions. At first, the method tries to delay the start time  $t_s$  of collision trajectories as the UAVs can

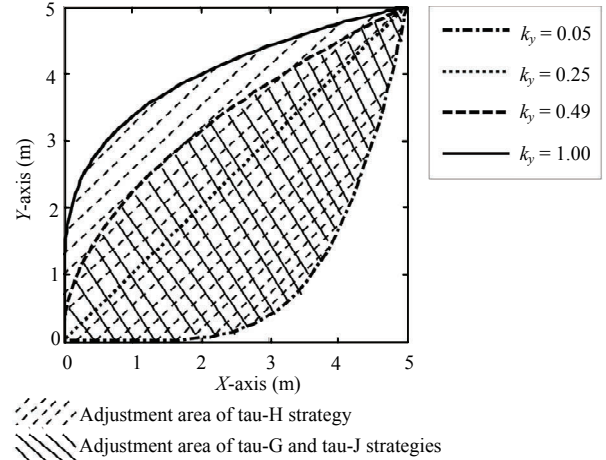


**Fig. 5** Shape adjustment areas of trajectories generated by different tau strategies.

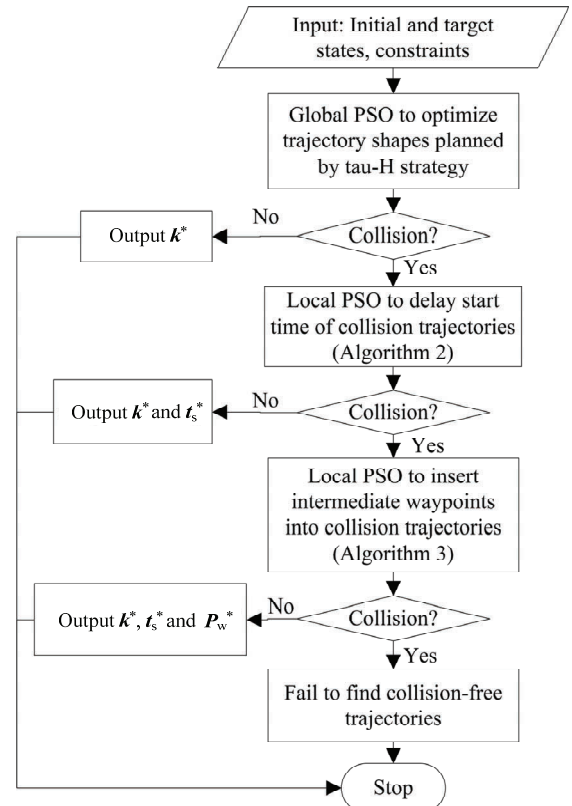


**Fig. 6** Flow chart of tau-H-PSO.

be regarded as time-variant obstacles. A local PSO is applied only on collision trajectories to obtain  $\mathbf{k}^*$  and the optimal start time  $t_s^*$ . If all collisions are resolved, the tau-H-PSO is finished. Otherwise some intermediate waypoints are inserted into the collision trajectories. The trajectory parameters including  $\mathbf{k}^*$ ,  $t_s^*$  and the optimal waypoints  $\mathbf{P}_w^*$  are also solved by the local PSO. The following subsections details this method.

#### 4.1 Collision detection based on PAZ

In tau-H-PSO, a geometric collision detection algorithm based on PAZ is adopted. PAZ is a geometric shell<sup>[24-26]</sup> around the UAV to keep the safe distance from obstacles. The safe distance should be selected by considering the horizontal and vertical security, the shape of UAV, and the disturbance such as wind and tracking errors.

As shown in Fig. 7, the ellipsoidal PAZ is utilized for collision detection in this paper. The PAZ is defined in the body-fixed frame **B** ( $O_b, X_b, Y_b, Z_b$ ), and the major and minor axes of the ellipsoid go along with the  $X_b$ -axis and  $Z_b$ -axis respectively. If the inequality expression Eq. (13) is fulfilled, there will be a collision alarm.  $D$  denotes the diameter of the circle in  $X_b$ - $Y_b$  plane,  $L$  is the length of the minor axis, and  $(X_{br}, Y_{br}, Z_{br})$  represents the coordinate of the obstacle relative to the center of UAV.

$$\frac{X_{br}^2 + Y_{br}^2}{D^2 / 4} + \frac{Z_{br}^2}{L^2 / 4} < 1. \quad (13)$$

The superiority of the ellipsoidal PAZ is the symmetry around the  $Z_b$ -axis. If  $D = L$ , or the pitch and roll of the UAV are sufficiently small in trajectory tracking, it is unnecessary to transform the PAZ from **B** to the navigation frame **N** in detection. Therefore, the symmetry of the ellipsoidal PAZ can greatly improve the detection efficiency.

#### 4.2 4D Trajectory generation algorithm

The optimization problem of 4D trajectory generation for  $N_{\text{UAV}}$  UAVs is given as

$$\begin{aligned} \min J &= \sum_{i=1}^{N_{\text{UAV}}} L_i \\ \text{s.t. } & \sum_{i=1}^{N_{\text{UAV}}} \sum_{\substack{j=1 \\ j \neq i}}^{N_{\text{UAV}}} C_{ij} = 0 \\ & v_{im} < v_{\max} \quad i = 1 \dots N_{\text{UAV}}; m = X, Y, Z \\ & a_{im} < a_{\max} \quad i = 1 \dots N_{\text{UAV}}; m = X, Y, Z \end{aligned} \quad (14)$$

The optimization objective  $J$  is to find a group of 4D trajectories with minimum length, in which  $L_i$  is the length of the  $i^{\text{th}}$  trajectory. The most important constraint is that the trajectories are collision-free. The collision matrix is defined as  $\mathbf{C} = [C_{ij}]_{N_{\text{UAV}} \times N_{\text{UAV}}}$ , in which  $C_{ij}$  denotes the collision between the  $i^{\text{th}}$  and  $j^{\text{th}}$  trajectories. As the position and velocity guided by

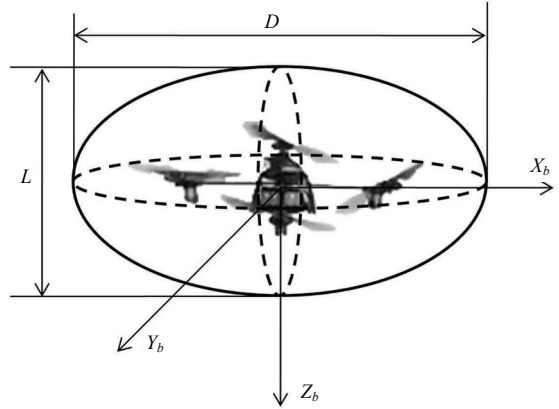


Fig. 7 Ellipsoidal PAZ.

tau-H strategy are synchronously planned in accordance with the arrival time, the arrival time constraint is not considered in this problem. Meanwhile, the dynamic constraints of UAVs including  $v_{\max}$  and  $a_{\max}$  are included. The velocity and acceleration along  $m$  axis of the  $i^{\text{th}}$  UAV are represented by  $v_{im}$  and  $a_{im}$  respectively.

Particularly, if the  $i^{\text{th}}$  trajectory composed of  $M_i$  segments needs to meet the total arrival time  $T_i$ , the constraint in Eq. (15) should be considered to ensure that the sum of the arrival time  $T_{ij}$  meets the total time constraint.

$$\sum_{j=1}^{M_i} T_{ij} = T_i \quad i = 1 \dots N_{\text{UAV}}. \quad (15)$$

According to Eq. (14), the cost function of  $N_{\text{UAV}}$  trajectories is defined as the linear weighted sum of the optimal objective and constraints, given as

$$f = \sum_{i=1}^{N_{\text{UAV}}} L_i + \omega_c f_c + \omega_v f_v + \omega_a f_a + \omega_T f_T, \quad (16)$$

where, symbols  $\omega_c$ ,  $\omega_v$ ,  $\omega_a$  and  $\omega_T$  are the weights of collision, velocity, acceleration, and total arrival time constraints, and  $f_c$ ,  $f_v$ ,  $f_a$  and  $f_T$  are the penalties for unfulfilled constraints.

##### 4.2.1 4D trajectory optimization

The modified PSO with dynamic inertia weight scheduling<sup>[27]</sup> (Algorithm 1) is applied to optimize the 4D trajectories. PSO is a bionic optimization algorithm developed from the behavior of fish school<sup>[28]</sup>. In this algorithm,  $N$  particles move in solution space to find the global optimal solution. PSO is iterative, and the solution improves with successive iterations. In the  $m^{\text{th}}$  it-

eration, the velocity  $v_i(m)$  and the position  $p_i(m)$  of the  $i^{\text{th}}$  particle are updated by considering both the local best solution  $pBest_i(m)$  and the global best solution  $gBest$ , given as

$$\begin{aligned} v_i(m+1) &= \omega \cdot v_i(m) + \varphi_1 \cdot rand \cdot (pBest_i(m) - p_i(m)) \\ &\quad + \varphi_2 \cdot rand \cdot (gBest - p_i(m)) \\ p_i(m+1) &= p_i(m) + v_i(m+1) \quad i = 1 \dots N \\ \omega &= \omega_{\max} - \frac{m(\omega_{\max} - \omega_{\min})}{IterMax}, \end{aligned} \quad (17)$$

where, the notation  $\omega$  is the inertia weight,  $\varphi_1$  and  $\varphi_2$  denote the local rate and global rate respectively,  $rand$  is a random number with uniform  $U(0,1)$  distribution, and  $IterMax$  represents the maximum iteration number.

If  $k_i$  and  $T_i$  of the  $i^{\text{th}}$  trajectory are optimized in PSO simultaneously,  $T_i$  should be normalized first to obtain the same range with the elements of  $k_i$ . The normalization undergoes a linear transformation with  $f(x) = bx + c$ , in which  $b$  and  $c$  are calculated as

$$\begin{cases} b = \frac{k_{\max} - k_{\min}}{T_{\max} - T_{\min}} \\ c = \frac{T_{\max}k_{\min} - T_{\min}k_{\max}}{T_{\max} - T_{\min}} \end{cases}. \quad (18)$$

#### 4.2.2 Collision resolution approaches

If the global optimization fails to find collision-free 4D trajectories, the CR approaches are adopted. To improve CR efficiency, only the collision trajectories are replanned. Although the parameters of these trajectories are locally optimized by PSO with the objective in Eq. (16), the whole group of trajectories is near-optimal.

##### (1) Delay the Start Time of movement (CR-DST)

CR-DST tries to resolve collisions only in the time dimension, which is specially designed for collision avoidance of 4D trajectories. As CR-DST is simple but efficient, it has been widely used in civil aviation<sup>[29]</sup>. If the start time of the trajectory is delayed to  $t_s$  ( $t_s > 0$ ), the arrival time is changed to  $T' = T - t_s$ . Hence the delayed trajectory should be replanned. As depicted in Algorithm 2, after the initialization of collision matrix  $C$ , the algorithm loops until there is no conflict or all collision trajectories have been replanned. In every loop, the delayed start time  $t_{si}^*$  and  $k_i^*$  of the most dangerous trajectory  $i$  are solved by local PSO. If the collisions cannot be avoided by CR-DST, a more effective approach is applied.

---

#### Algorithm 1 The modified PSO algorithm

---

```

1 For  $i^{\text{th}}$  particle ( $i = 1 \dots N$ ) do
2     Randomly initialize  $p_i$  and  $v_i$ 
3     Initialize  $pBest_i \leftarrow p_i$ 
4     If  $f(pBest_i) < f(gBest)$  then
5          $gBest \leftarrow pBest_i$ 
6     End if
7 End for
8 Repeat
9 For  $i^{\text{th}}$  particle ( $i = 1 \dots N$ ) do
10    Update  $v_i$  and  $p_i$  as Eq. (17)
11    If  $f(p_i) < f(pBest_i)$  then
12         $pBest_i \leftarrow p_i$ 
13        If  $f(pBest_i) < f(gBest)$  then
14             $gBest \leftarrow pBest_i$ 
15        End if
16    End if
17 End for
18 Until  $IterMax$  or the termination criterion is met

```

---

#### Algorithm 2 Delay the start time of movement (CR-DST)

---

```

1 Initialize the collision matrix  $C$ 
2 Repeat
3     Find out trajectory  $i$  with the most conflicts
4     Obtain  $k_i^*$  and  $t_{si}^*$  by PSO
5     If collisions of trajectory  $i$  are avoided, then
6         Update parameters of trajectory  $i$ 
7         Detect conflicts and update matrix  $C$ 
8     End if
9 Until collision-free or all collision trajectories are replanned

```

---

##### (2) Insert Intermediate Waypoints (CR-IIW)

CR-IIW, as shown in Fig. 8, can avoid collisions in both spatial and temporal dimensions. Though the intermediate waypoints can be planned by geometric methods, it is still difficult to obtain the optimal coordinates of waypoints  $P_w^*$  and the matched trajectory parameters. Therefore,  $P_w$  is also optimized by the local PSO. If  $N_w$  waypoints are inserted into  $i^{\text{th}}$  trajectory, the trajectory consists of  $N_w+1$  segments. So the constraint in Eq. (19) should be considered to ensure that the total flight time is shorter than  $T_i$ .

$$\sum_{j=1}^{N_w+1} T_{ij} \leq T_i \quad i = 1 \dots N_{\text{UAV}}. \quad (19)$$

Before optimization,  $T_{ij}$  and  $P_w$  should be normalized. According to Algorithm 3, only one waypoint is inserted into the collision trajectory at first, and then the approach loops to resolve collisions as shown in steps

4–11. If all collision trajectories have been replanned but there are still collisions, the approach will increase  $N_w$  by 1, and repeat the resolution process.

## 5 Simulation results

More than 1,800 simulations have been carried out to validate the performance of tau-H-PSO. For comparison, the same simulations are handled by the method with tau-G strategy (tau-G-PSO)<sup>[29]</sup> and a conventional method using one-at-a-time strategy (OAAT-PSO)<sup>[24]</sup>. The OAAT strategy can guide the UAVs to pass the collision point one after another. As this strategy is simple but efficient, it is widely used in conflict resolution for cooperative systems<sup>[24,30]</sup>. In the two contrasting methods, the trajectories are optimized by PSO as well.

As far as we know, there is no standard benchmark to verify the 4D trajectory generation method for multi-UAVs<sup>[30]</sup>. So it is important to adopt convincing simulations to validate the proposed method. In this paper, the simulations are developed in a scenario with 2 to 10 homogeneous UAVs working in the same cubic space, whose side is 30 m. The dynamic constraints of UAVs are  $v_{\max} = 5 \text{ m}\cdot\text{s}^{-1}$  and  $a_{\max} = 2 \text{ m}\cdot\text{s}^{-2}$ . The safe distance between different UAVs is 1 m. Considering the trajectory tracking errors, the spherical PAZ with a radius of 1.5 m is adopted for collision detection.

In this scenario, the UAVs cooperatively complete a series of simultaneous arrival missions. Particularly, the vehicles first fly from the initial position to a common middle point, and then simultaneously arrive at destinations. The initial positions, middle point and destinations are chosen arbitrarily, and the parking time at the middle point is ignored. One of the scenarios with five UAVs is shown in Fig. 9, in which the middle point is marked with M, and the destinations are numbered from G1 to G5. All the simulations are designed using MATLAB R2013a and completed on a laptop with a 2.6 GHz Core i5-3230M CPU and 4 GB of RAM.

### (1) Simulations of the global trajectory optimization

The global optimization of trajectory shape adjustment is the major procedure of tau-H-PSO, and has a great effect on the performance of the whole method. In this part, only the global PSO iterates 100 times to solve each test case. Fig. 10 shows the convergence of tau-H-PSO by the reduction of the mean normalized cost<sup>[24]</sup> with the number of iterations ( $N_{\text{iter}}$ ). Table 1

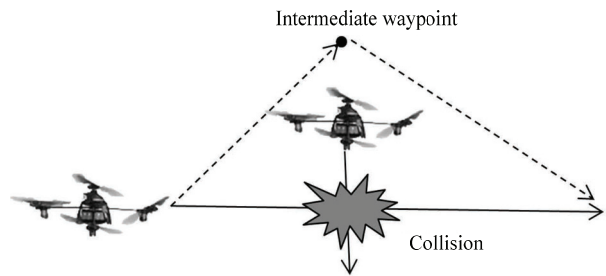


**Fig. 8** Scenario of a primary conflict resolved by CR-IIW.

### Algorithm 3 Insert intermediate waypoints (CR-IIW)

```

1 Initialize  $N_w = 1$ 
2 Repeat
3   Initialize the collision matrix  $\mathbf{C}$ 
4   Repeat
5     Find out trajectory  $i$  with the most collisions
6     Obtain  $\mathbf{P}_{wi}^*$ ,  $t_{si}^*$  and  $k_i^*$  by PSO
7     If collisions of trajectory  $i$  are avoided, then
8       Update parameters of trajectory  $i$ 
9     Detect conflicts and update matrix  $\mathbf{C}$ 
10    End if
11 Until collision-free or all collision trajectories are replanned
12 Increase  $N_w$  by 1
13 Until collision-free or maximum  $N_w$  is met

```

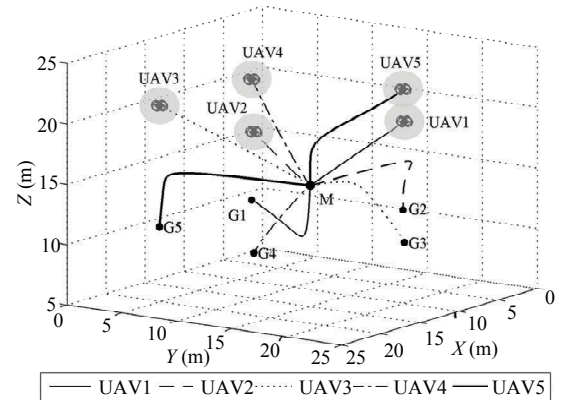


**Fig. 9** Scenario with 5 UAVs and the tracking results of trajectories given by tau-H-PSO.

shows a comparison among  $N_{\text{iter}}$  of different methods when the normalized cost reduces 90%. From this table,  $N_{\text{iter}}$  increases with  $N_{\text{UAV}}$ . But when numerous UAVs crowd in the workspace, the growth of  $N_{\text{iter}}$  slows down. The reason for this phenomenon is two-fold. Firstly, when  $N_{\text{UAV}}$  becomes larger, the problem of Eq. (14) is harder to optimize. Secondly, if  $N_{\text{UAV}}$  is significantly large, the difference between the maximum and minimum costs becomes smaller as no collision-free solu-

tions are found in global PSO. By contrast,  $N_{\text{iter}}$  of tau-H-PSO is smaller than that of the other methods, and the slowdown of  $N_{\text{iter}}$  growth comes later. The results indicate that the convergence of tau-H-PSO is better.

The mean time of 100 global iterations is shown in Fig. 11, in which the curves of tau-H-PSO and tau-G-PSO are almost the same. As the trajectories given by OAAT-PSO are straight lines without the need for integration in the length calculation, it works faster than tau-based methods.

## (2) Simulations of the whole 4D trajectory generation method

To validate the performance of the whole tau-H-PSO method, a termination criterion is designed for PSO. If no better solutions are found in the following five iterations after obtaining collision-free trajectories, the optimization will be finished. The total number of test cases is 100, and  $\text{IterMax} = 150$ . Four key results depending on  $N_{\text{UAV}}$  are shown in Fig. 12. The percentage of cases solved ( $Pct_{\text{solv}}$ ) in global optimization is shown in Fig. 12a and mean number of global iterations ( $N_{\text{iter}}$ ) cost for one case is shown in Fig. 12b. The  $Pct_{\text{solv}}$  in CR approaches are separately displayed in Fig. 12c (CR-DST) and Fig. 12d (CR-IIW).

From Fig. 6, the flow chart of tau-H-PSO and tau-G-PSO is the global optimization of trajectories, CR-DST, and CR-IIW. But as the OAAT strategy allows the UAV waiting at its initial position, the global OAAT-PSO is a combination of the global optimization and CR-DST. Hence there is no curve for OAAT-PSO in Fig. 12c. The cases that cannot be solved in global OAAT-PSO are only handled by CR-IIW. If collision-free trajectories are achieved in one stage, the following procedures will not be executed. Therefore, the larger  $Pct_{\text{solv}}$  in global optimization means the fewer cases are solved by CR approaches, which demonstrates that the trajectory generation method has a better CR capability.

From Fig. 12a, when the density of UAVs increases,  $Pct_{\text{solv}}$  in global optimization decreases, and obtaining collision-free trajectories needs more iterations. Compared with tau-G-PSO, tau-H-PSO can solve more cases with smaller  $N_{\text{iter}}$ . When compared with the OAAT-PSO, the performance of tau-H-PSO should take the effect of CR-DST in Fig. 12c into consideration, because the global OAAT-PSO contains the function of CR-DST. From Figs. 12a and 12c, we can draw a conclusion that

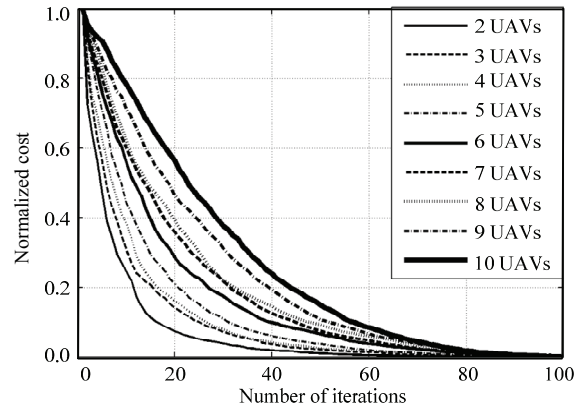


**Fig. 10** Reduction of the mean normalized cost with successive iterations.

**Table 1**  $N_{\text{iter}}$  in global PSO when the normalized cost reduced 90%

$N_{\text{UAV}}$	2	3	4	5	6	7	8	9	10
OAAT-PSO	15	28	44	59	71	71	70	73	70
tau-G-PSO	12	26	38	43	56	60	61	63	63
tau-H-PSO	15	26	27	31	40	45	48	52	57

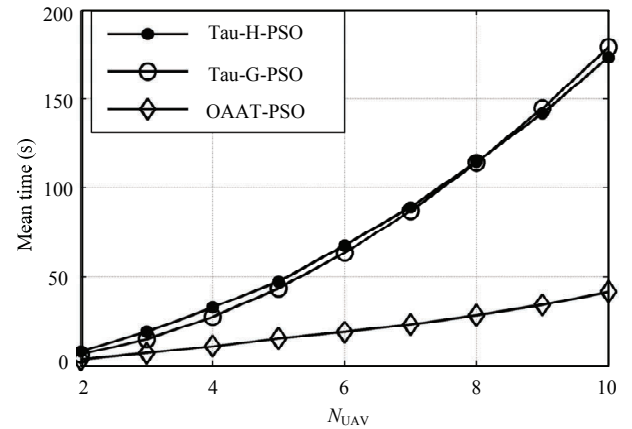


**Fig. 11** Mean execution time depending on  $N_{\text{UAV}}$ .

tau-H-PSO performs better than OAAT-PSO.

Figs. 12c and 12d show the performance of CR approaches. As depicted in Fig. 12c, the CR-DST approach of tau-H-PSO resolves more collision cases than tau-G-PSO. Because most test cases are solved in global PSO and CR-DST, as shown in Fig. 12d, the percentage of problems ultimately resolved by CR-IIW of tau-H-PSO is significantly smaller. The results in Fig. 12 indicate that our proposed method has a better CR capability than that of the other methods, especially in the cases with more UAVs. As all the test cases are successfully solved by tau-H-PSO, the validity of the CR approaches is demonstrated.

### (3) Simulations of 4D trajectory tracking

To validate the flyability of trajectories, the simulations of 4D trajectory tracking are carried out with the kinematics and dynamics models of five quad-rotors<sup>[31]</sup>. The tracking results of trajectories generated by tau-H-PSO are shown in Fig. 9. To make the simulation results more visualized, a virtual reality scenario is designed, and a video of this flight is shown at [www.youtube.com/watch?v=STUGC0diTsA&feature=youtu.be](http://www.youtube.com/watch?v=STUGC0diTsA&feature=youtu.be).

Unfortunately, this paper cannot display the details

of all UAVs, so the tracking results of the most dangerous trajectories are provided. Coincidentally, the most dangerous trajectory of every method is the trajectory for UAV3. The distances between UAV3 and others are shown in Fig. 13, in which the thick dashed line is the minimum safe distance. All the trajectories are collision-free but the dangerous distance of the trajectory generated by OAAT-PSO maintains more time. The results show that the tau-H-PSO can generate safer trajectories with enough tolerance to tracking errors.

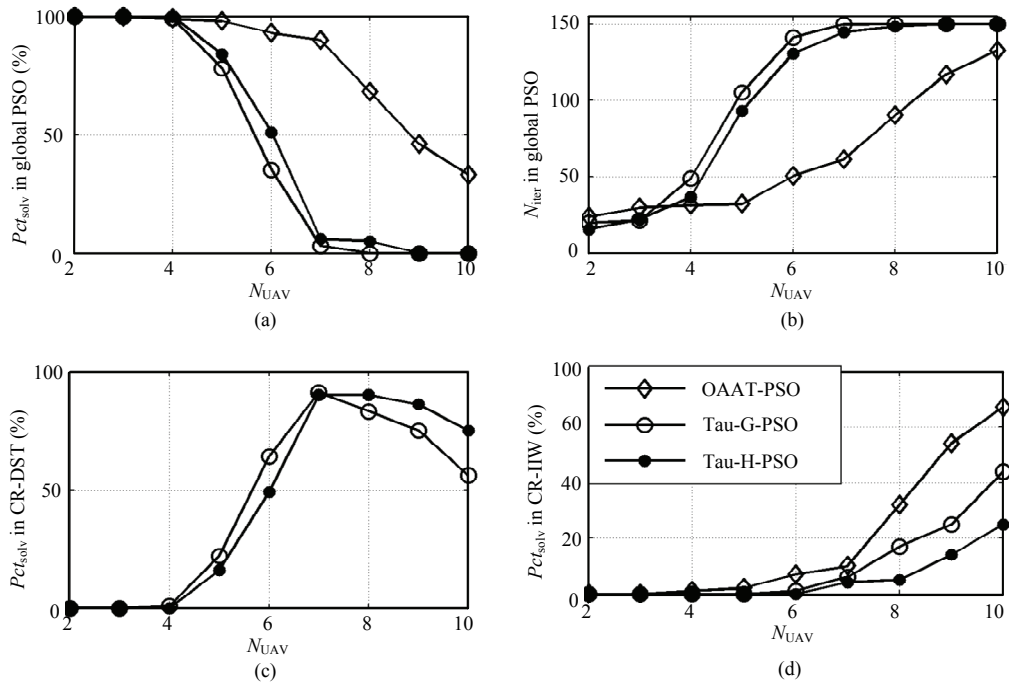


**Fig. 12** Performance of the whole trajectory generation methods depending on  $N_{UAV}$ : (a)  $Pct_{solv}$  in global PSO; (b)  $N_{iter}$  cost in global PSO; (c)  $Pct_{solv}$  in CR-DST; (d)  $Pct_{solv}$  in CR-IIW.

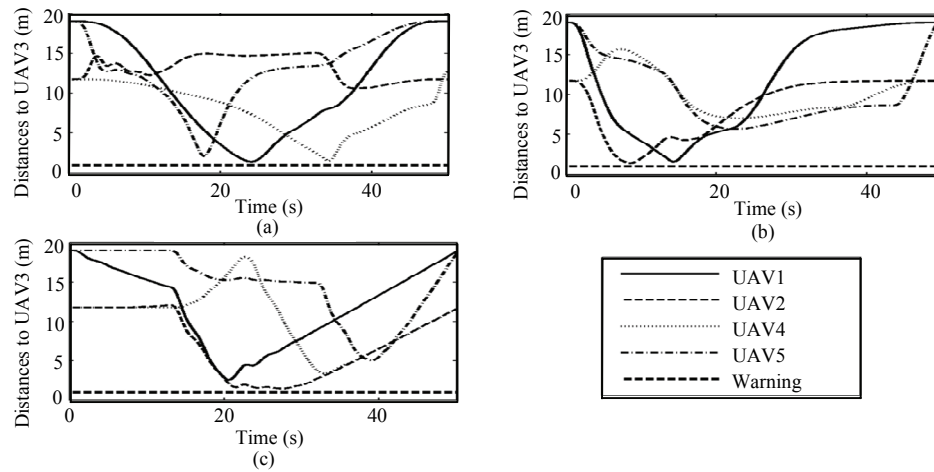


**Fig. 13** Distances between the most dangerous UAV and others: (a) Tau-H-PSO; (b) tau-G-PSO; (c) OAAT-PSO.

For UAV3, the horizontal trajectories and tracks near the initial position and the middle point are shown in Fig. 14, and the pitch, roll, and thrust are shown in Fig. 15. In the tracking process of the trajectory planned

by tau-H-PSO, the track, attitudes and thrust of UAV3 are much smoother, and the tracking errors are smaller. These results indicate that tau-H-PSO can generate more flyable 4D trajectories than that of the other methods.

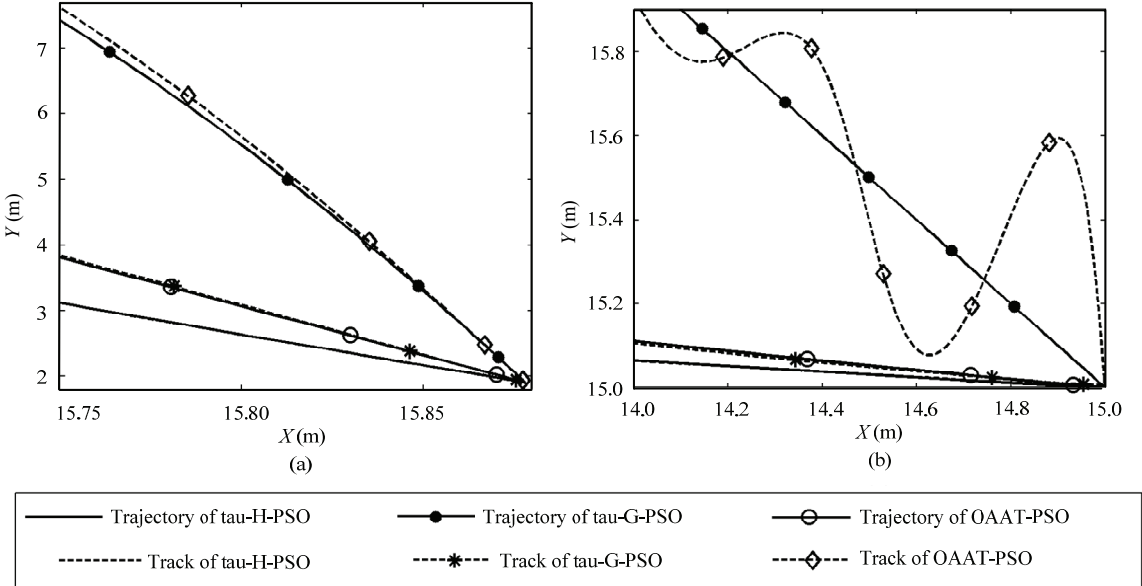


**Fig. 14** Partial horizontal trajectories and tracks: (a) Near the initial position; (b) near the middle point.

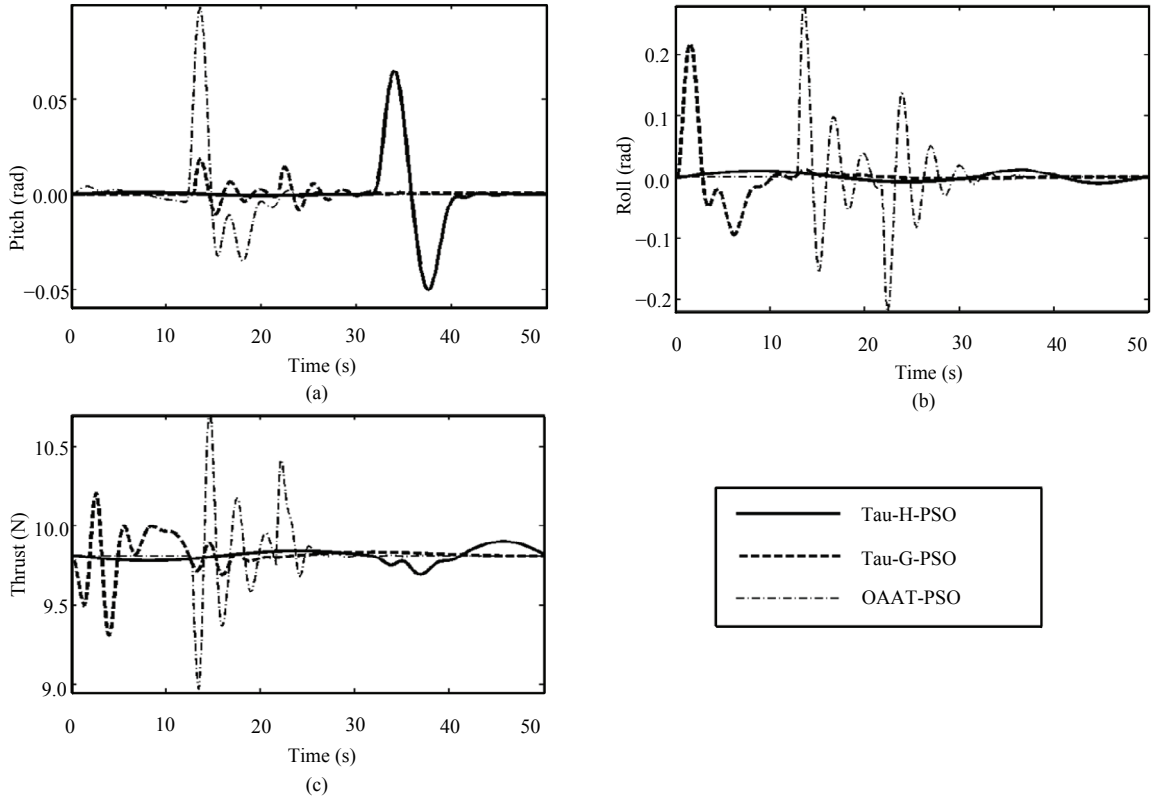


**Fig. 15** (a) Pitch, (b) roll and (c) thrust of UAV3.

## 6 Conclusion

This paper presents a collision-free 4D trajectory generation method (tau-H-PSO) for multi-UAVs based on the bio-inspired tau-H strategy and PSO algorithm. The tau-H strategy is proposed on the basis of the general tau theory and harmonic motion. In tau-H-PSO, we apply the tau-H strategy to plan 4D trajectories, and utilize the modified PSO to optimize trajectory parameters. To guarantee the flight safety, collision detection and resolution approaches are adopted to avoid conflicts. The main advantage of tau-H-PSO is the proposition of the tau-H strategy and its application in multi-UAV scenarios. Benefit from this strategy, the 4D trajectory can fit to guide the movement with zero initial acceleration. Furthermore, the trajectory achieves a stronger shape adjustment capability, which is helpful for de-confliction in the applications of UAVs. Numerous simulations are carried out to demonstrate that tau-H-PSO has a better convergence and a stronger CR capability, and can provide more flyable and safer 4D trajectories than the existing methods. Our future work aims at performing real-time experiments to validate the performance of the presented method.

## Acknowledgment

This work is supported by the National Natural Science Foundation of China under Grant No. 61004066 and Zhejiang Provincial Natural Science Foundation under Grant No. LY15F030005. Meanwhile, we also extend our thanks to the School of Aeronautics and Astronautics of Zhejiang University for consistent support.

## References

- [1] Makhdoom I H, Qin S Y. Simultaneous arrival of multiple UAVs under imperfect communication. *Aircraft Engineering and Aerospace Technology*. 2012, **84**, 37–50.
- [2] Kendoul F. Survey of advances in guidance, navigation, and control of unmanned rotorcraft systems. *Journal of Field Robotics*. 2012, **29**, 315–378.
- [3] Ru C J, Wei R X, Wang Y Y, Che J. Multimodel predictive control approach for UAV formation flight. *Mathematical Problems in Engineering*, 2014, **2014**, 1–11.
- [4] Yoshinori M, Takeshi T. 4D trajectory optimization in the presence of uncertainty. *Aviation Technology, Integration, and Operations Conference*, Los Angeles, CA, 2013, 1–11.
- [5] Swenson H, Barhydt R, Landis M. Next Generation Air Transportation System (NGATS), Air Traffic Management (ATM)-airport project, NASA, 2006.
- [6] Ruiz S, Piera M A, Nosedal J, Ranieri A. Strategic de-confliction in the presence of a large number of 4D trajectories using a causal modeling approach. *Transportation Research Part C: Emerging Technologies*, 2014, **39**, 129–147.
- [7] Oh H, Turchi D, Kim S, Tsourdos A, Pollini L, White B. Coordinated standoff tracking using path shaping for multiple UAVs. *IEEE Transactions on Aerospace and Electronic Systems*, 2014, **50**, 348–363.
- [8] Shanmugavel M, Tsourdos A, Zbikowski R, White B A, Rabath C A, Lechevin N. A solution to simultaneous arrival of multiple UAVs using Pythagorean Hodograph curves. *Proceedings of the American Control Conference*, Minnesota, USA, 2006, 2813–2818.
- [9] Berry A J, Howitt J, Gu D W, Postlethwaite L. A continuous local motion planning framework for unmanned vehicles in complex environments. *Journal of Intelligent & Robotic Systems*. 2011, **66**, 477–494.
- [10] Bousson K, Machado P F F. 4D trajectory generation and tracking for waypoint-based aerial navigation. *WSEAS Transactions on Systems & Control*, 2013, **8**, 105–119.
- [11] Degen S C, Alvarez L M, Ford J J, Walker R A. Tensor field guidance for time-based waypoint arrival of UAVs by 4D trajectory generation. *IEEE Aerospace Conference*, Big Sky, Montana, USA, 2009, 1–7.
- [12] Wu P Y, Campbell D, Merz T. Multi-objective four-dimensional vehicle motion planning in large dynamic environments. *IEEE Transactions on Systems, Man, and Cybernetics, Part B: Cybernetics*, 2011, **41**, 621–634.
- [13] Goerzen C, Kong Z, Mettler B. A survey of motion planning algorithms from the perspective of autonomous UAV guidance. *Journal of Intelligent & Robotic Systems*, 2010, **57**, 65–100.
- [14] Lee D N, Reddish P E. Plummeting gannets: A paradigm of ecological optics. *Nature*, 1981, **293**, 293–294.
- [15] Lee D N, Davies M N, Green P R. Visual control of velocity of approach by pigeons when landing. *Journal of Experimental Biology*, 1993, **180**, 85–104.
- [16] Jump M, Padfield G D. Investigation of the flare maneuver using optical tau. *Journal of Guidance, Control, and Dynamics*, 2006, **29**, 1189–1200.
- [17] Lee D N. General tau theory: Evolution to date. *Perception*, 2009, **38**, 837–858.
- [18] Zhang Z, Zhang S, Xie P, Ma O. Bioinspired 4D trajectory generation for a UAS rapid point-to-point movement. *Journal of Bionic Engineering*, 2014, **11**, 72–81.

- [19] Kendoul F, Ahmed B. Bio-inspired TauPilot for automated aerial 4D docking and landing of unmanned aircraft systems. *Proceedings of the IEEE/RSJ International Conference on Intelligent Robots and Systems (IROS)*, Vilamoura, Algarve, Portugal. 2012, 480–487.
- [20] Kendoul F. Four-dimensional guidance and control of movement using time-to-contact: Application to automated docking and landing of unmanned rotorcraft systems. *The International Journal of Robotics Research*, 2014, **33**, 237–267.
- [21] Zhang Z, Xie P, Ma O. Bio-inspired trajectory generation for UAV perching movement based on tau theory. *International Journal Advanced Robotic System*, 2014, **11**, 1–13.
- [22] Chiang Y-J, Klosowski J T, Lee C, Mitchell, J S B. Geometric algorithms for conflict detection/resolution in air traffic management. *Proceedings of the 36th IEEE Conference on Decision and Control*, San Diego, California. 1997, 1835–1840.
- [23] Lee D N. A theory of visual control of braking based on information about time-to-collision. *Perception*, 1976, **5**, 437–459.
- [24] Alejo D, Cobano J A, Heredia G, Ollero A. Collision-free 4D trajectory planning in Unmanned Aerial Vehicles for assembly and structure construction. *Journal of Intelligent & Robotic Systems*, 2014, **73**, 783–795.
- [25] Goss J, Rajvanshi R, Subbarao K. Aircraft conflict detection and resolution using mixed geometric and collision cone approaches. *AIAA Guidance, Navigation, and Control Conference and Exhibit*, Providence, Rhode Island, 2004, 1–20.
- [26] Barnier N, Allignol C. Trajectory deconfliction with constraint programming. *The Knowledge Engineering Review*, 2012, **27**, 291–307.
- [27] Shi Y, Eberhart R C. Parameter selection in particle swarm optimization. *Proceedings of the Evolutionary Programming VII*, 1998, 591–600.
- [28] James K, Russell E. Particle swarm optimization. *Proceedings of the IEEE International Conference on Neural Networks*, Perth, WA, 1995, 1942–1948.
- [29] Yang Z Q, Fang Z, Li P. A bio-inspired collision-free 4D trajectory generation method for unmanned aerial vehicles based on tau theory. *34th Chinese Control Conference (CCC)*, Hangzhou, Zhejiang, China, 2015, 6961–6968.
- [30] Alejo D, Cobano J, Heredia G, Ollero A. Particle swarm optimization for collision-free 4d trajectory planning in unmanned aerial vehicles. *Proceedings of the International Conference on Unmanned Aircraft Systems (ICUAS)*, Atlanta, USA, 2013, 298–307.
- [31] Corke P. *Robotics, Vision and Control: Fundamental Algorithms in MATLAB*, 1st ed, Springer, Berlin, 2011.